



Stabilization of salt hydrates using flexible polymeric networks

Joey Aarts^{a,b}, Bas van Ravensteijn^c, Hartmut Fischer^d, Olaf Adan^{b,d}, Henk Huinink^{a,b,*}

^a Eindhoven Institute of Renewable Energy Systems, Eindhoven University of Technology, PO Box 513, Eindhoven, 5600, MB, the Netherlands

^b Transport in Permeable Media Group, Department of Applied Physics, Eindhoven University of Technology, PO Box 513, Eindhoven, 5600, MB, the Netherlands

^c Department of Pharmaceutics, Utrecht Institute for Pharmaceutical Sciences (UIPS), Utrecht University, Universiteitsweg 99, 3584, CG, Utrecht, the Netherlands

^d TNO Materials Solution, High Tech Campus 25, Eindhoven, the Netherlands

ARTICLE INFO

Handling Editor: L Luo

Keywords:

Energy storage
Salt hydrates
Stabilization
Polymers
Calcium oxalate
Potassium carbonate

ABSTRACT

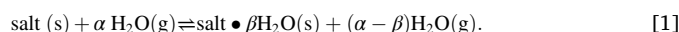
The use of salt hydrates for thermochemical energy storage is associated with mechanical instabilities during cyclic hydration/dehydration. On the other hand, some salt hydrates do not suffer from these drawbacks, but manufacturing of mm-sized particles is still a challenge. In this work a one pot synthesis method is presented which results in composites using poly (dimethyl siloxane) (PDMS) as binder. Energy densities of 1.14 GJ/m³ and 0.67 GJ/m³ are achieved for a K₂CO₃ and CaC₂O₄ composite, respectively. Swelling upon hydration decreases compared to non-stabilized particles. The best K₂CO₃ composite shows mechanical stability for at least 35 cycles, and the average power output at 50 % conversion increases with cycling to 50–55 kW/m³ at 20 °C and 33 % relative humidity. Also, a stable CaC₂O₄ composite is made suitable for heat storage. The particle volume and hydration kinetics remain constant for at least 20 cycles. An average power output at 50 % conversion of 5 kW/m³ at 20 °C and 33 % relative humidity is generated. The results from this work show how a one-pot fabrication method can be used to obtain mm-sized particles with enhanced mechanical stability during cycling. Stabilization can be achieved independent of the salt hydrate solubility or material properties.

1. Introduction

Since fossil fuels still account for 64 % of the global energy use for building related heating, a shift towards renewable energy is needed [1]. Renewable energy sources, such as solar and wind energy, are location and time-dependent, resulting in a non-synchronized energy supply and demand. To overcome this problem energy needs to be stored during peak supply and can be released during peak demand.

Thermal energy storage can be used to store the excess energy produced in abundant times until demanding times are present, where the energy can be released directly in the form of heat. Thermochemical energy storage can store energy in a loss-free manner. Therefore, successful energy storage and release can be realized in timescales from hours until months.

Salt hydrates are a promising class of thermochemical materials for energy storage in the built environment. Salt hydrates release heat once subjected to water vapor (hydration) and store energy once excess heat is supplied (dehydration). The reversible reaction proceeds as follows



Here α [–] and β [–] represent the stoichiometric coefficients of the reaction.

For a successful application of salt hydrates in a packed bed heat battery, the salt must be manufactured into mm-sized particles instead of powder. Manufacturing into larger particles is necessary to prevent a large pressure drop over the reactor bed [2]. A major challenge associated with using salt hydrates is that they undergo swelling, fracturing, and cracking with cycling [3,4]. Therefore, the material needs to be stabilized. In addition to that, some salt hydrates do not suffer from these drawbacks, but manufacturing of mm-sized particles is still a challenge. In this work a successful method to manufacture mechanically stable mm-sized particle for both types of materials is presented.

One promising salt hydrate for thermochemical energy storage, identified by Donkers et al. (2017), is potassium carbonate [5]. It was selected based on various aspects, such as energy density, safety, costs, and user conditions. In addition, a recent study by Wang et al. (2022) has identified promising use cases for application of K₂CO₃ inside a

* Corresponding author. Eindhoven Institute of Renewable Energy Systems, Eindhoven University of Technology, PO Box 513, Eindhoven, 5600, MB, the Netherlands.

E-mail addresses: j.aarts@tue.nl (J. Aarts), b.g.p.vanravensteijn@uu.nl (B. van Ravensteijn), hartmut.fischer@tno.nl (H. Fischer), olaf.adan@tno.nl (O. Adan), h.p.huinink@tue.nl (H. Huinink).

<https://doi.org/10.1016/j.energy.2023.129540>

Received 18 July 2023; Received in revised form 17 October 2023; Accepted 30 October 2023

Available online 3 November 2023

0360-5442/© 2023 The Authors. Published by Elsevier Ltd. This is an open access article under the CC BY license (<http://creativecommons.org/licenses/by/4.0/>).

(particle packed bed) heat battery for Dutch residential houses [6].

Another promising salt, which is less extensively investigated, is CaC_2O_4 for which the powder shows good cyclic hydration stability, has a high deliquescence relative humidity, and produces output temperatures $>100^\circ\text{C}$ [7–9]. Another key advantage of this salt is its low volumetric change during hydration and dehydration based on the crystal densities ($2.22\text{ g}\cdot\text{cm}^{-3}$ and $1.97\text{ g}\cdot\text{cm}^{-3}$ for the hydrous and anhydrous crystal density respectively [10,11]), as such reducing the mechanical stresses and swelling during cycling. Possible use-cases for CaC_2O_4 have been recently identified as well [7].

Several successful methods have been reported in literature to stabilize K_2CO_3 . Ravensteijn et al. (2021) used encapsulation with a polymeric shell (cellulose derivatives) for mechanical stabilization [12]. The packed bed energy density of the encapsulated material ($0.65\text{ GJ}\cdot\text{m}^{-3}$) was equal to the packed bed energy density of the uncoated particles ($0.66\text{ GJ}\cdot\text{m}^{-3}$) due to the low amount of polymer required. Even though a decrease in kinetics was not found due to the polymer encapsulation, salt hydrate particles with faster kinetics might lose power output once encapsulation is applied. This effect was observed when the authors coated zeolite using cellulose derivatives.

Impregnation into vermiculite resulted in successful cyclic stabilization and offered possibilities to use the deliquescence transition for heat storage as well [13,14]. Stabilization inside a highly porous polymer resulted in higher power output compared to pure salt hydrate mm-sized particle [15]. Even though achieving successful mechanical stabilization, the hydration energy density is lowered significantly in the case of a salt in a porous matrix (from $1.3\text{ GJ}\cdot\text{m}^{-3}$ on crystal level to $0.3\text{--}0.5\text{ GJ}\cdot\text{m}^{-3}$ on various composite levels).

The major disadvantage of the discussed encapsulation and impregnation methods is that they are multi-step processes. Encapsulation is preceded by a particle manufacturing step followed by coating and an energy intensive drying step. This energy intensive drying step is also required after the impregnation step when using impregnation methods.

Considering CaC_2O_4 , formation of mm-sized particles, required for the target application, is extremely difficult. This is due to the small powder size because of low solubility in most solvents and fast crystallization. Additionally, due to the low solubility impregnation into a porous host matrix is not possible. Therefore, to the knowledge of the authors, no mechanically stable mm-sized particle (under cyclic loading) for this material has been reported in literature until now.

In this work a one-pot stabilization procedure is presented using poly (dimethyl siloxane), PDMS, in combination with uniaxial pressing. The advantage of a one-pot synthesis is the absence of a drying step, simplicity of the production process and a manufacturing price reduction. Using uniaxial pressing, particles with high energy densities can be obtained compared to impregnation methods. The PDMS binder is added to provide mechanical integrity to salt hydrate particles and enable the manufacturing of stable mm-sized particles of salt hydrates with low solubility.

The potential of using PDMS and polymer composites has been illustrated in recent literature.

Salviati et al. (2019) demonstrated the effect of adding poly diallyl dimethylammonium chloride (PDAC) to flat cylindrical SrBr_2 particles [16]. By incorporation of PDAC the mechanical stability and hydration kinetic both improved. Using sodium alginate well defined beads filled with CaCl_2 could be produced [17,18]. The proposed synthesis route proved to be scalable, flexible, and the well-defined shape is suitable for packed bed applications. The composite showed stable cyclic performance for at least 5 cycles. The concept of using PDMS for stabilization of salt hydrates has been investigated using MgSO_4 and LiCl [19,20]. The authors prepared a slurry of the precursor material, catalyst, and salt hydrate, which is then molded and dried in an oven. The flexibility of the matrix resulted in mechanical stabilization of the salt hydrate. However, detailed cyclic analysis has not yet been performed.

PDMS has good chemical and thermal stability while exhibiting elastic properties, high elongation at break and high water vapor permeability [21,22]. The used PDMS-salt mixtures can cure at room temperature once mixed, which enables a one-pot fabrication of well-defined mm-sized stabilized particles. The geometry of the stabilized particles is similar to non-stabilized mm-sized particles reported in previous literature [23].

Extensive cyclic testing is performed on PDMS- $\text{K}_2\text{CO}_3\cdot 1.5\text{H}_2\text{O}$ composites of varying compositions by varying the base powder size and PDMS concentration. In addition, cyclic testing of a PDMS- $\text{CaC}_2\text{O}_4\cdot\text{H}_2\text{O}$ composite is presented as well. Using the stabilization method reported in this work, for the first time a mechanically stable mm-sized $\text{CaC}_2\text{O}_4\cdot\text{H}_2\text{O}$ composite under cyclic loading is manufactured, suitable for thermochemical energy storage.

2. Materials and methods

2.1. Materials and material preparation

PDMS Sylgard 184 base material and curing agent were obtained from DOW. $\text{K}_2\text{CO}_3\cdot 1.5\text{H}_2\text{O}$ was provided by Evonik Functional Solutions GmbH. $\text{K}_2\text{CO}_3\cdot 1.5\text{H}_2\text{O}$ was milled (Fritsch planetary ball mill) and sieved into a $300\text{--}500\text{ }\mu\text{m}$ and $50\text{--}300\text{ }\mu\text{m}$ fraction. $\text{CaC}_2\text{O}_4\cdot\text{H}_2\text{O}$ ($<50\text{ }\mu\text{m}$ fraction) was purchased from Thermo Fisher Scientific and used without further treatment.

2.2. Particle fabrication

Sylgard 184 base material and curing agent were mixed in a 10:1 ratio (as recommended by the product technical datasheet) together with a specific amount of the desired salt hydrate in hydrated state ($\text{K}_2\text{CO}_3\cdot 1.5\text{H}_2\text{O}$ or $\text{CaC}_2\text{O}_4\cdot\text{H}_2\text{O}$). The mixture was thoroughly mixed by hand into a paste until a uniform consistency was reached. Pressing of cylindrical particles ($\sim 12.5\text{ mm}$ diameter, $\sim 2\text{ mm}$ in height) was done from the paste and was performed using a PO-Weber PW-40 2 column press with varying pressures ($1\text{--}9\text{ kbar}$). The particles were then left to cure at 20°C and 33 % relative humidity (RH) (saturated MgCl_2 solution [24]) for 72 h. The density of the particles was measured by dividing the salt weight m_s [g] of the particle by the geometrically measured volume V_t [cm^3] (Mitutoyo digital caliper). The precise salt and binder weight fraction (of the total particle weight) within the particle were determined from the water uptake during the first hydration cycle, neglecting the water uptake by the PDMS matrix.

The relative salt densities of pristine and cycled K_2CO_3 - and CaC_2O_4 PDMS particles were calculated by dividing the measured density ρ_m [$\text{g}\cdot\text{cm}^{-3}$] by the theoretical crystal density ρ_t [$\text{g}\cdot\text{cm}^{-3}$] as follows

$$\rho_{\text{rel}} = \frac{\rho_m}{\rho_t} = \frac{(m_s/V_t)}{\rho_t} \quad [1]$$

The theoretical densities for hydrous and anhydrous K_2CO_3 were taken as $2.18\text{ g}\cdot\text{cm}^{-3}$ and $2.43\text{ g}\cdot\text{cm}^{-3}$, respectively [25,26]. For CaC_2O_4 $2.22\text{ g}\cdot\text{cm}^{-3}$ and $1.97\text{ g}\cdot\text{cm}^{-3}$ were taken for the hydrous and anhydrous crystal density, respectively [10,11]. The absolute error in density measurements is estimated to be 0.01 [-] (1 % when the density is expressed in percentages).

2.3. Kinetic measurements

Dehydration was performed overnight in an oven at 130°C and 160°C for $\text{K}_2\text{CO}_3\cdot 1.5\text{H}_2\text{O}$ and $\text{CaC}_2\text{O}_4\cdot\text{H}_2\text{O}$ composites, respectively. Full dehydration was confirmed by measuring the weight loss. Hydration was performed at 20°C and 33 % RH (saturated MgCl_2 solution [24]) inside a desiccator until full conversion was reached. The anhydrous particles were placed inside the desiccator with one side (bottom) covered from water vapor. The particle weight was recorded by briefly

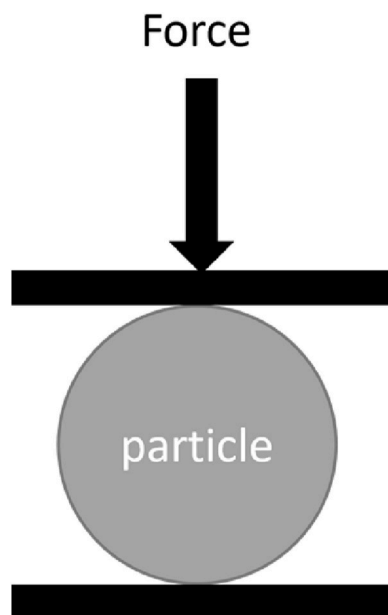


Fig. 1. Schematic illustration of performed compression tests on cylindrical mm sized particles.

Table 1

Results of various binder concentrations and pressing pressures using 50–300 μm K_2CO_3 powder.

Manufacturing pressure	<5 wt % binder	5 wt % binder	8 wt % binder
1 kbar	Inhomogeneous mix:	successful	successful
3 kbar	degradation during first		
9 kbar	cycle		Sticky particles: difficult to manufacture

taking it from the desiccator, weighting and putting it back with the same side down as before. To ensure a homogenous distribution of water vapor a small ventilator was placed inside the desiccator. The energy density ED [$\text{J} \cdot \text{m}^{-3}$] is defined as the energy density of a single composite particle

$$ED = \frac{n_t \cdot \Delta H}{V_t} \quad [2]$$

Here n_t [mol] and ΔH [$\text{J} \cdot \text{mol}^{-1}$] represent the total number of reacted moles of water and the associated enthalpy, respectively.

2.4. Compression tests

Compressive tests are performed at a compressive strain rate of $0.5 \text{ mm} \cdot \text{min}^{-1}$ on a Shimadzu autograph (AGS-X-series). For measurements, the cylindrical particle is placed on its curved side (Fig. 1). Otherwise, when placed on its flat side, the applied force would exceed the device pressure limits. Snapshots of the compressive process were obtained using a Dino Lite digital camera.

2.5. Scanning electron microscopy (SEM)

SEM analysis was performed on a FEI Quanta 600 using 10 kV and low vacuum measurements to reduce charge accumulation on the sample. Prior to imaging, the samples were cryogenically fractured to obtain a clean fracture surface. This is done by freezing the samples in liquid nitrogen followed by breaking them by hand. This procedure gave samples with a clear fracture plane to facilitate imaging of the internal structure of the composites.

3. Results and discussion

3.1. K_2CO_3 - PDMS: Influence of manufacturing pressure and binder concentration

First the effect of manufacturing conditions (binder concentration and manufacturing pressure) on the K_2CO_3 -PDMS particle mechanical integrity and PDMS distribution were investigated. The results are given in Table 1.

From Table 1 it can be seen that a minimum weight percentage of binder is required to form stable PDMS-salt particles. A binder concentration of less than 5 wt% resulted in particle degradation during the first hydration. This degradation is most probably caused by the inhomogeneous distribution of binder resulting in different rates of expansion. When using 8 wt % of binder, only the preparation of particles while applying lower manufacturing pressures was successful. At high pressures (9 kbar) the particles became very sticky, and it was difficult to remove the particles from the pressing tool. Therefore, binder concentrations above 8 wt % were not further investigated. When using 5 wt % of binder successful manufacturing of particles was possible for the full range of manufacturing pressures (1–9 kbar).

To verify that a continuous PDMS network throughout the particle interior has been formed, a particle was placed in demineralized water to dissolve the salt. The particle was kept in water for 4 weeks to verify the integrity of the PDMS network and completely dissolve the salt. The SEM images show an empty intact sponge like structure (Fig. 2). Note that the sponge structure has been compressed during drying and handling and therefore a denser structure appears.

The effect of the PDMS on the mechanical integrity compared to non-stabilized (pure salt) particles was investigated using compression tests. The results of a compression test of a stabilized and non-stabilized

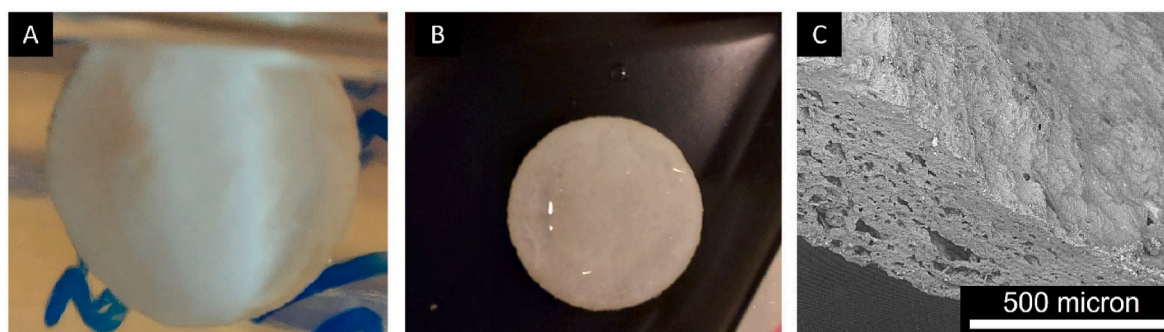


Fig. 2. A salt-PDMS particle made from 50 to 300 powder with 5 wt % binder made at 1 kbar in water to dissolve the salt, showing the empty matrix in water (A), once taken out of the water (B) and a SEM image of the empty PDMS binder dried a 40°C (C).

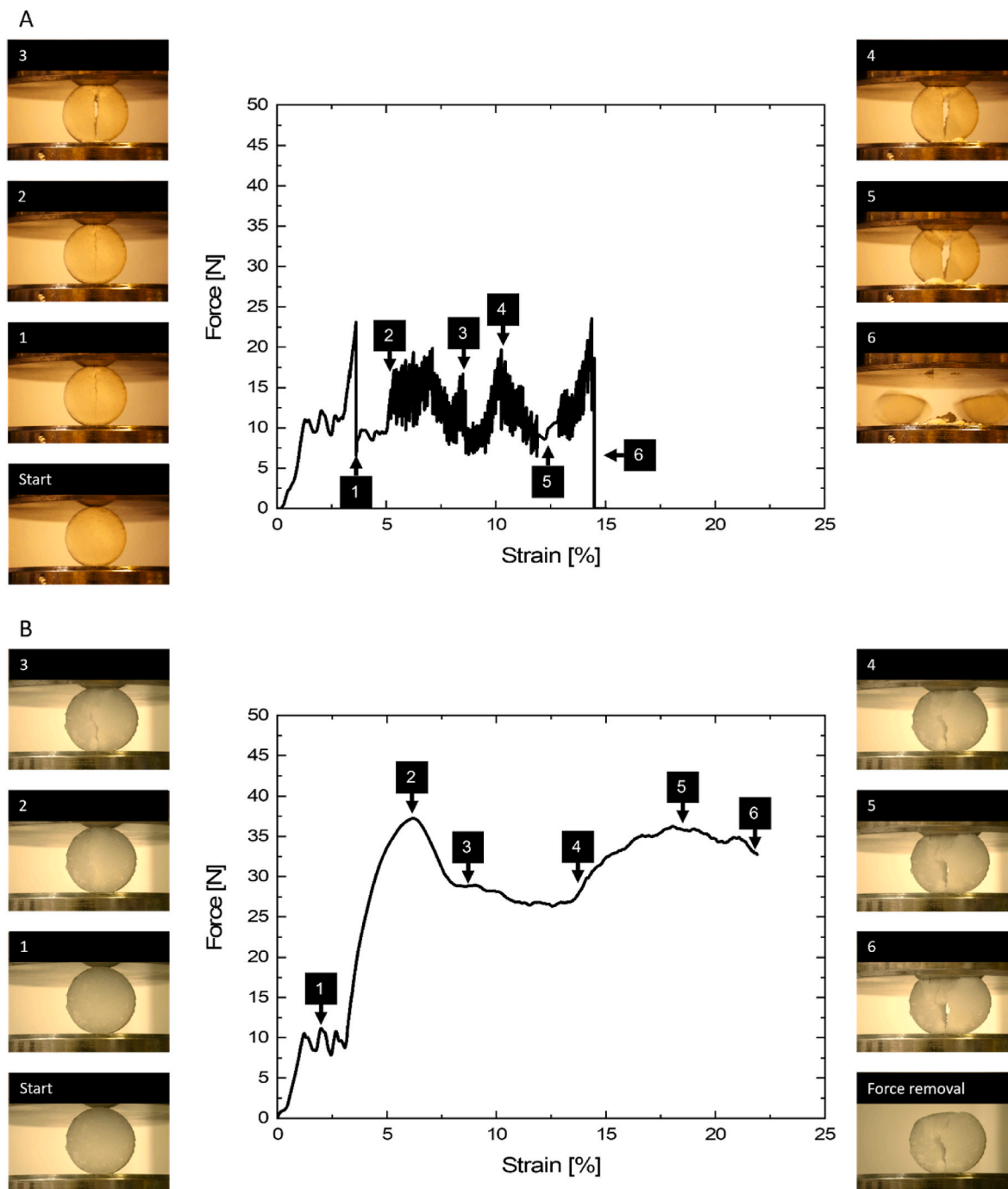


Fig. 3. Compression test on a non-stabilized particle (A) and stabilized PDMS-K₂CO₃ particle (B). Both particles were pressed from 50 to 300 μ m powder and have a relative density of 80 %. The PDMS-salt particle contains 5 wt % PDMS. The absolute error in density measurements is estimated to be 0.01 [-] (1 % when the density is expressed in percentages).

particle are given in Fig. 3.

The non-stabilized particle shows similar behavior as observed in earlier work, in which a particle with lower relative density shows continuous cracking during compression [4,27]. During this continuous cracking, the particle continuously loses powder and eventually above 15 % compressive strain, the particle splits in two halves.

In the case of the stabilized particle a different behavior is observed. After 3 % compression a steep increase in force is observed. The steep increase in force until 37 N is due to the elastic deformation of the PDMS matrix. After this steep increase (6 % compression) the first crack appears, resulting in a decrease in force. Subsequently, additional force is

required to compress the particle further, but no powder is lost from the particle due to the action of the PDMS matrix. When the force is removed the particle partially recovers its shape and does not split in two halves, even though a major crack has formed throughout the particle. This illustrates the increased mechanical integrity due to the PDMS network.

Next, the effect of manufacturing pressure on PDMS distribution and particle morphology was investigated. By varying the manufacturing pressure between 1 and 9 kbar it was found that the relative salt density of the PDMS particles (with equal binder content) did not vary significantly, in contrast to particles without binder [23]. This is most probably due to the incompressibility of the PDMS binder.

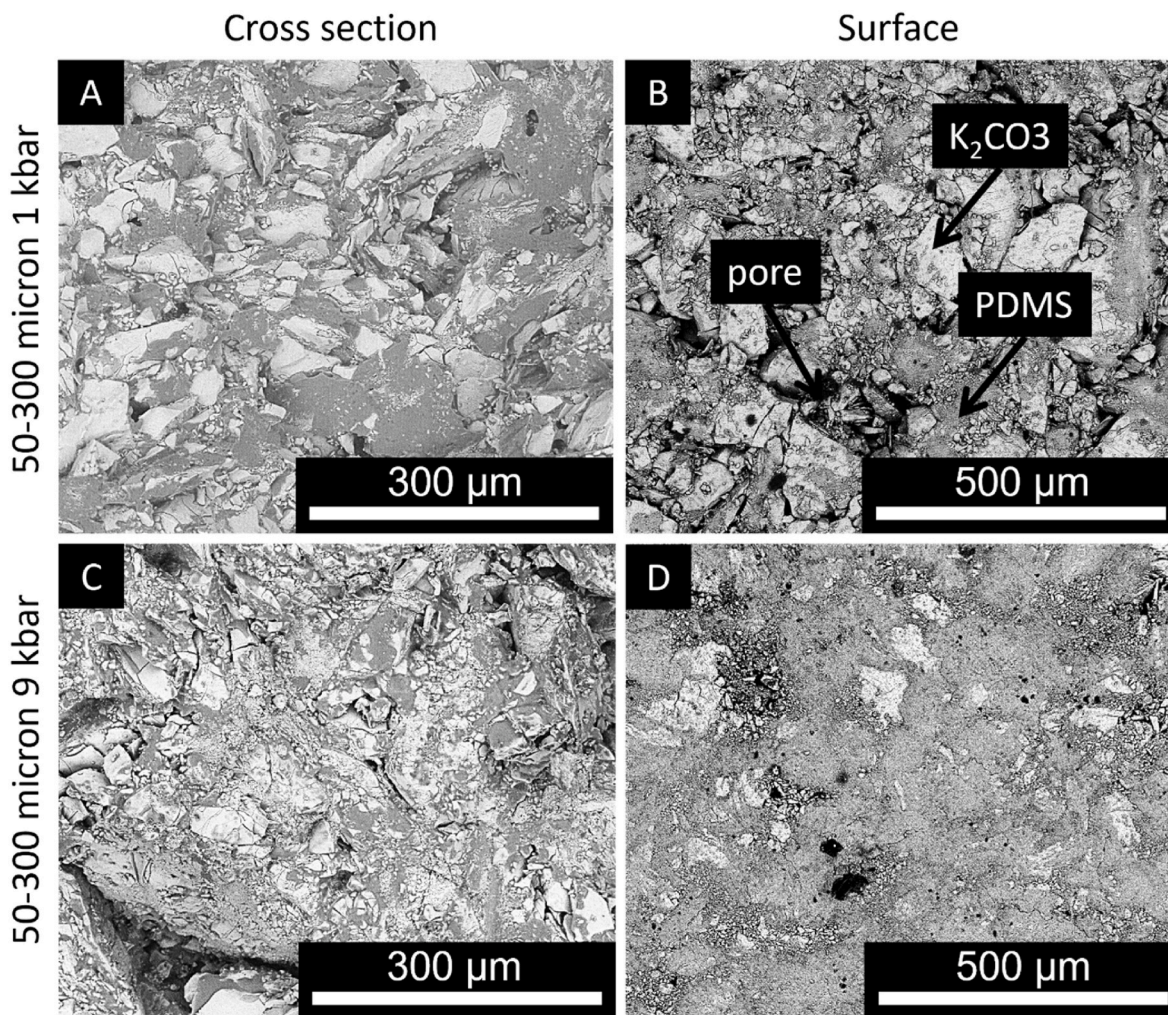


Fig. 4. Cross section (A and C) and surface (B and D) SEM images of pristine K_2CO_3 -PDMS particles made from a 50–300 μm powder fraction with 5 wt % binder at 1 and 9 kbar manufacturing pressure. The grey and white colors represent the PDMS and $K_2CO_3 \cdot 1.5H_2O$, respectively.

Table 2

Number of stable cycles for particles made from 50 to 300 μm powder, various manufacturing pressures and 5 wt % binder. Hydration was performed at 33 % RH, 20 $^{\circ}C$ and dehydration overnight in an oven at 130 $^{\circ}C$.

Manufacturing pressure	Stable cycles		
	5 wt % binder	8 wt % binder	Non stabilized reference
1 kbar	33	At least 35	11
3 kbar	17	16	–
9 kbar	9	–	–

SEM imaging shows that the manufacturing pressure does influence the PDMS distribution within the particles. Fig. 4 shows the PDMS distribution on the surface and within particles made with different manufacturing pressures. The grey and white colors represent the PDMS and $K_2CO_3 \cdot 1.5H_2O$, respectively.

Both manufacturing pressures (1 and 9 kbar) resulted in an internal PDMS structure partially covering the salt grains. However, using a higher pressure more binder is pressed outwards towards the particle surface resulting in less binder available to form the internal network structure.

To investigate the effect of binder concentration and manufacturing pressure on the particle mechanical stability, cyclic dehydration at 130 $^{\circ}C$ in an oven, followed by hydration at 33 % RH and 20 $^{\circ}C$ in a

desiccator was performed. Particles made with various binder concentrations and manufacturing pressures were evaluated. The number of stable cycles until complete fracture of the particle is given in Table 2. A reference particle made of pure salt was measured as well.

For both binder concentrations (5 and 8 wt %) a decrease in the number of stable cycles with increasing manufacturing pressure is observed. At 3 kbar manufacturing pressure no significant difference is found between the two binder concentrations. For the lowest manufacturing pressure, the particle with 8 wt % binder was still stable after 35 cycles. Both binder concentrations performed better compared to the non-stabilized reference particle. Pressing a particle at 1 kbar with 8 wt % binder resulted in an energy density of $1.14 \text{ GJ} \cdot \text{m}^{-3}$.

The effect of decreased cyclic stability with increasing manufacturing pressure most probably originates from the distribution of PDMS in the particles changing with manufacturing pressure, as observed by SEM (Fig. 4). Since higher manufacturing pressures resulted in less internal PDMS, the stabilizing effect decreased. Since the particles pressed at 1 kbar showed the highest cyclic stability, only a detailed analysis of particles pressed at 1 kbar is presented (Fig. 5).

For both binder concentrations (5 wt % and 8 wt %) the average volume increase compared to the starting material is similar over cycles until an inflection point is observed (10 % per cycle). After this inflection point, again a similar average slope is observed for both samples (2–3%). All slopes before and after this inflection point be approximated by a linear fit (black lines in Fig. 5). However, the slopes before the inflection

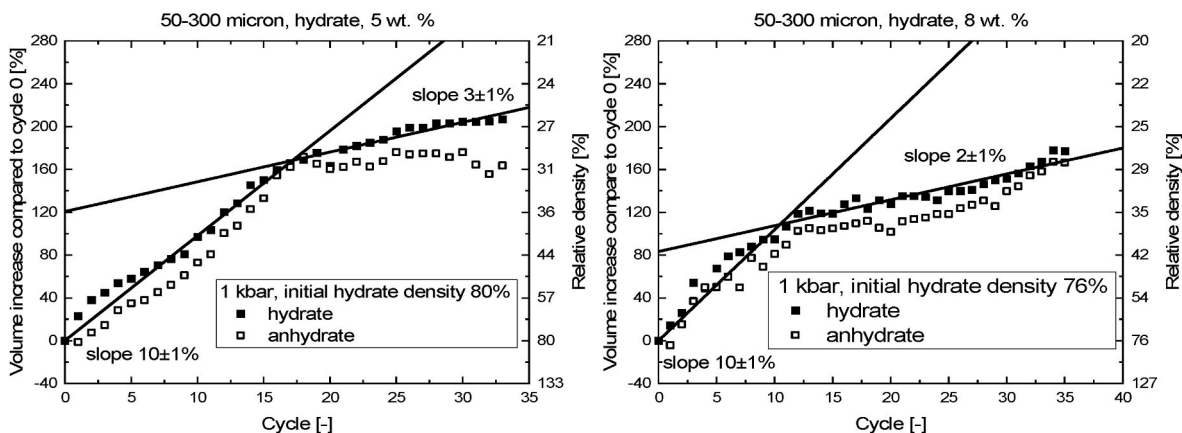


Fig. 5. Volume increases compared to the pristine hydrate particle for particles made from 50 to 300 μm powder, 1 kbar manufacturing pressures and 5 or 8 wt % binder. Hydration was performed at 33 % RH, 20 $^{\circ}\text{C}$ and dehydration overnight in an oven at 130 $^{\circ}\text{C}$. The initial density represents the relative hydrate salt density as produced. The black lines represent the linear fits through the 1 kbar sample in hydrated state before and after the inflection point. The slope for each line is given in the figure. The absolute error in density measurements is estimated to be 0.01 [-] (1 % when the density is expressed in percentages).

Table 3

Slopes and inflection points for particles made from 50 to 300 μm powder, 1 kbar manufacturing pressures and 5 or 8 wt % binder. Hydration was performed at 33 % RH, 20 $^{\circ}\text{C}$ and dehydration overnight in an oven at 130 $^{\circ}\text{C}$. A non-stabilized reference particle was measured as well. The absolute error in density measurements is estimated to be 0.01 [-] (1 % when the density is expressed in percentages).

Binder amount	Slope before inflection point [% per cycle]	Slope after inflection point [% per cycle]	Hydrate relative density at inflection point [%]
Non-stabilized reference	13	–	Not present
5 wt %	10	3	30
8 wt %	10	2	35

point are lower compared to a reference non-stabilized particles indicating that the swelling increase per cycle is decreased (Table 3).

SEM analysis has been performed on a sample prior to and after the inflection point. The particles were made from 50 to 300 μm powder, 5 wt % binder, and at a pressure of 1 kbar (Fig. 6). Fig. 6A shows the cross section after 10 dehydration/hydration cycles. It is observed that the PDMS changed into a web like structure compared to the sheets covering

the salt grains in Fig. 4A. Additionally, a porous structure is generated within the main grains which resembles recent literature observations [4]. Just after the inflection point (Fig. 6B and 18 cycles) the observed structure remains similar. However, the PDMS web like structure could no longer be observed. This is most probably due to the web like treads becoming very thin of being overgrown by the porous structure (no additional mass loss was observed).

For both samples, the inflection point is found around 35 % relative hydrate density. The precise point of the inflection point is difficult to determine due to the gradual transition. The inflection point is most probably the point at which the main grains within the particle underwent most of the required morphological changes (compare porous structures in Fig. 6). Due to a decrease in morphological changes fewer swelling forces occur, decreasing the swelling over cycles. Swelling over cycling does not completely stop after the inflection point due to the remaining volume changes caused by the density difference between hydrous and anhydrous material.

The volume increase at which the 5 wt % binder particle fractures is found to be 207 % which corresponds to a relative density of 26 %. For the 8 wt % binder particle cyclic stability was obtained for at least 35 cycles, however due to measurement time constraints cycling was stopped after 35 cycles. Based on the remaining density at which the 5 wt % particle fractured stability for at least 45–50 cycles is expected for

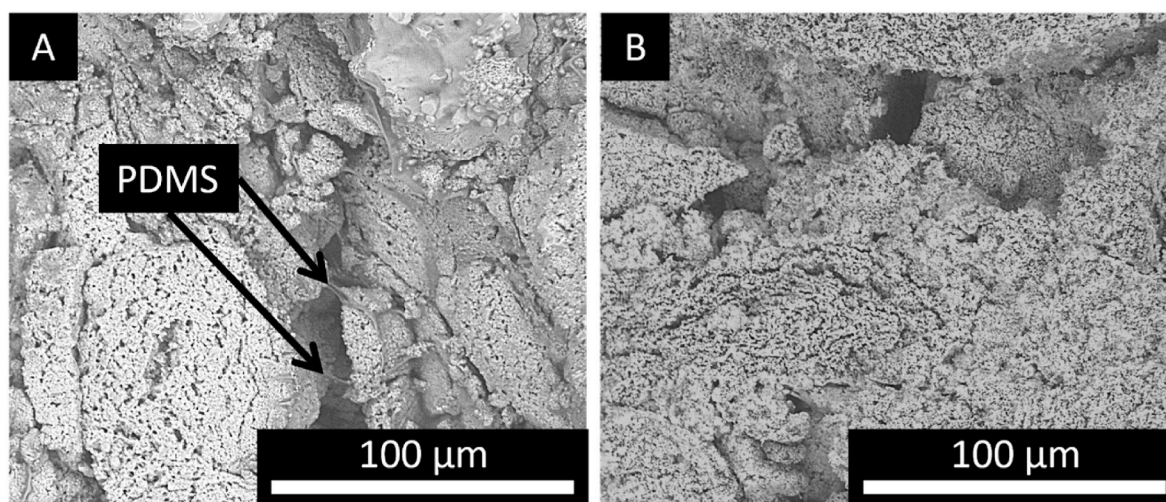


Fig. 6. Cross section SEM images of cycled K_2CO_3 -PDMS particles made from a 50–300 μm powder fraction with 5 wt % binder at 1 kbar manufacturing pressure before (A, 10 cycles) and after (B, 18 cycles) the inflection point.

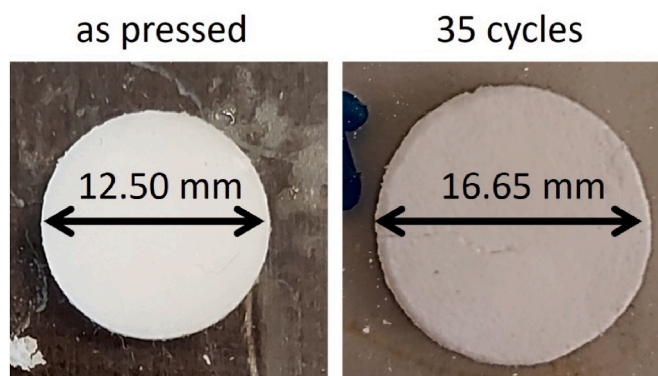


Fig. 7. Particle made from 50 to 300 μm powder at 1 kbar manufacturing pressures and 8 wt % binder before cycling (as pressed) and after 35 dehydration/hydration cycles.

the 8 wt % sample before mechanical destabilization occurs. Visual inspection of the 8 wt % sample shows minimal morphological changes. Only small surface cracks are found after 35 cycles compared to the as produced particle, indicating successful stabilization (Fig. 7).

3.2. K_2CO_3 - PDMS: Particle size effect

In addition to manufacturing pressure and binder concentration, the effect of the powder particle sizes was investigated. Since it was observed in section 3.1 that particles pressed at 1 kbar were the most stable upon cycling, only particles pressed at 1 kbar are discussed in the following section. The volume changes for the 300–500 μm powder fraction pressed at 1 kbar with 5 and 8 wt % binder are given in Fig. 8.

The initial average slopes are comparable for both wt. % of binder, though the slopes of the 8 wt % sample (10 %) being slightly higher compared to the 5 wt % sample (13 %) and the 8 wt % sample made from the 50–300 powder fraction (10 %).

The 5 wt % sample does not show an inflection point and fractures at a relative density of 24 % (Fig. 8). This value matches the density value (26 %) at which fracturing of the 5 wt % sample made from 50 to 300 μm powder occurs. The sample with 8 wt % binder shows an inflection point around a relative density of 35 %, similar to particles made from 50 to 300 μm powder. In Table 4 the inflection points and swelling slopes are given, and it is visible that both binder concentrations result in a decrease in swelling slope.

The absence of an inflection point in the particle containing 5 wt %

binder is most likely due to two reasons. First, the larger (primary) powder fraction requires more geometric grain changes (fracturing) to reach a stable (smaller) morphological state. Second, the salt-PDMS contact surface is lower after cycling due to the larger particle size fraction. When a large grain turns into an ensemble of smaller grains as found in previous work, only a part of the original grain will be connected to the PDMS [4]. Due to the lack of an inflection point, and decrease in slope, the swelling per cycle does not decrease. Therefore, fracturing occurs at an earlier cycle compared to the particle made from 50 to 300 μm powder.

Due to the higher amount of binder an inflection point does exist in the 8 wt % particle. The breakage point is found at 168 % volume increase which corresponds to a relative density of 28 % like the fracture density found for all other 1 kbar particles. Due to a higher slope after the inflection point, fracturing occurs at an earlier cycle compared to the particle made from 50 to 300 μm powder.

3.3. K_2CO_3 - PDMS: Hydration kinetics and cycling

Successful stabilization requires that the power output is not compromised (upon cycling). The hydration kinetics for particles made from 50 to 300 μm powder over several cycles is given in Fig. 9.

Obviously, the first cycle of the 8 wt % sample is significantly slower compared to the 5 wt % sample. In cycle 2, the kinetics have accelerated for both samples and at higher cycle numbers kinetic stabilization started to occur. This matches the observations from earlier work in which the increase in porosity results in an increase in hydration kinetics [4]. The slower kinetics of the 8 wt % sample is due to the increased PDMS concentration which affects the water vapor diffusion.

Table 4

Slopes and inflection points for particles made from 300–500 μm powder, 1 kbar manufacturing pressures and 5 or 8 wt % binder. Hydration was performed at 33 % RH, 20 °C and dehydration overnight in an oven at 130 °C. A non-stabilized reference particle from literature is included as well [4]. The absolute error in density measurements is estimated to be 0.01 [-] (1 % when the density is expressed in percentages).

Binder amount	Slope before inflection point [% per cycle]	Slope after inflection point [% per cycle]	Hydrate relative density at inflection point [%]
Non-stabilized reference [4]	15	–	Not present
5 wt %	10	–	Not present
8 wt %	13	5	34

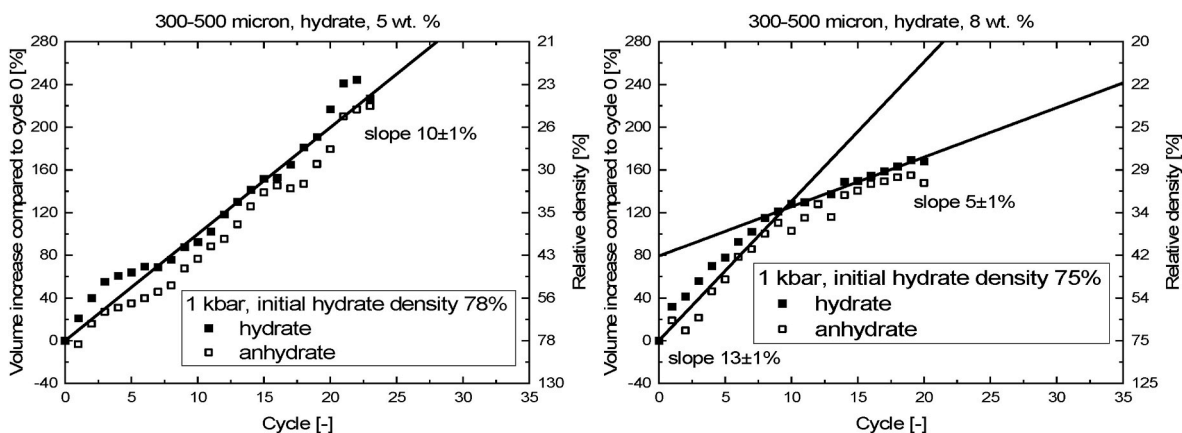


Fig. 8. Volume increases compared to the as produced hydrate particle for particles made from 300 to 500 μm powder, 1 kbar manufacturing pressures and 5 or 8 wt % binder. Hydration was performed at 33 % RH, 20 °C and dehydration overnight in an oven at 130 °C. The initial density represents the relative salt density as produced. The black lines represent the linear fits through the sample in hydrated state before and after the inflection point. The slope for each line is given in the figure. The absolute error in density measurements is estimated to be 0.01 [-] (1 % when the density is expressed in percentages).

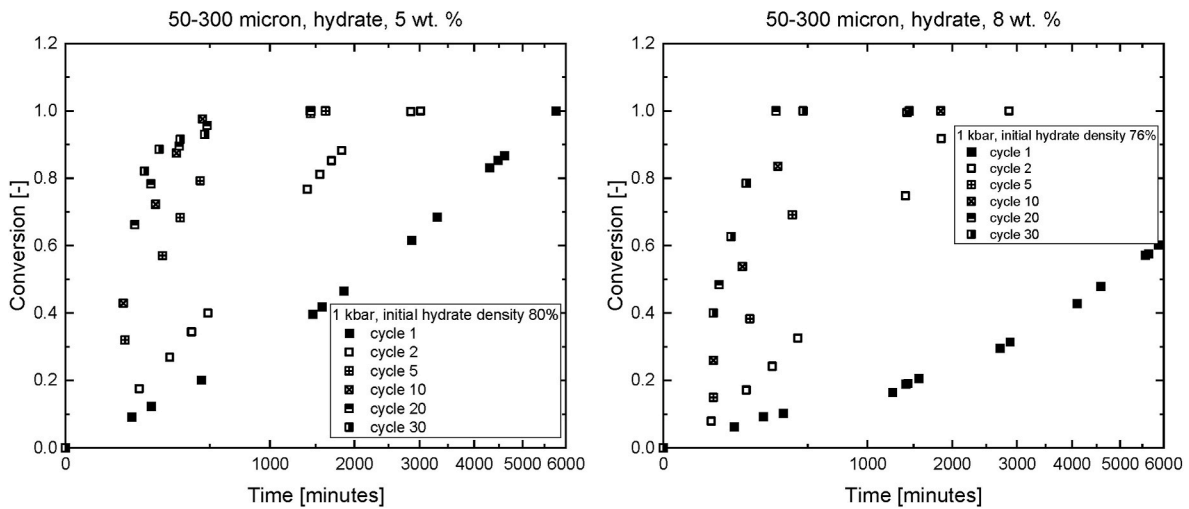


Fig. 9. Hydration conversion over time for various cycles for particles made from 50 to 300 μm powder, 1 kbar manufacturing pressures and 5 or 8 wt % binder. Hydration was performed at 33 % RH, 20 $^{\circ}\text{C}$ and dehydration overnight in an oven at 130 $^{\circ}\text{C}$. The given density represents the initial relative salt density at which the particle is produced. The absolute error in density measurements is estimated to be 0.01 [-] (1 % when the density is expressed in percentages).

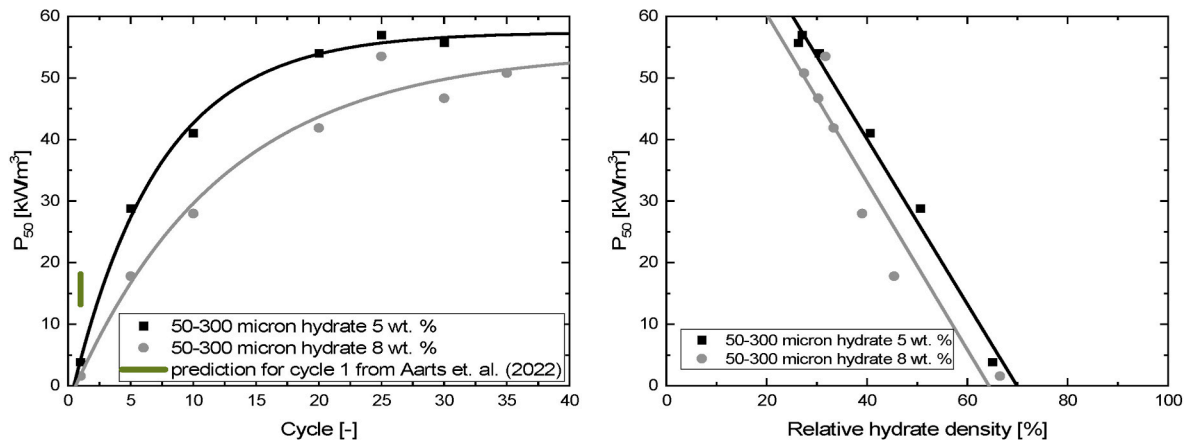


Fig. 10. Average power at 50 % conversion versus cycling and relative hydrate density for the particles cycled in Fig. 9. The green line represents the predicted range for the power output in cycle 1 from Aarts et al. (2022) [23].

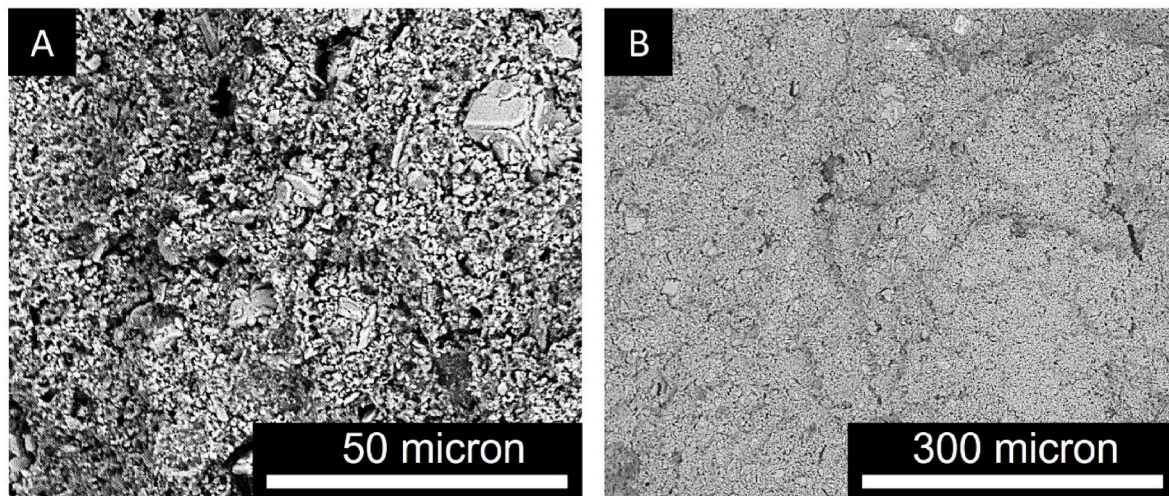


Fig. 11. Cross section SEM images of a CaC_2O_4 -PDMS particle made from a $<50 \mu\text{m}$ powder fraction with 39 wt % binder at 1 kbar manufacturing pressure.

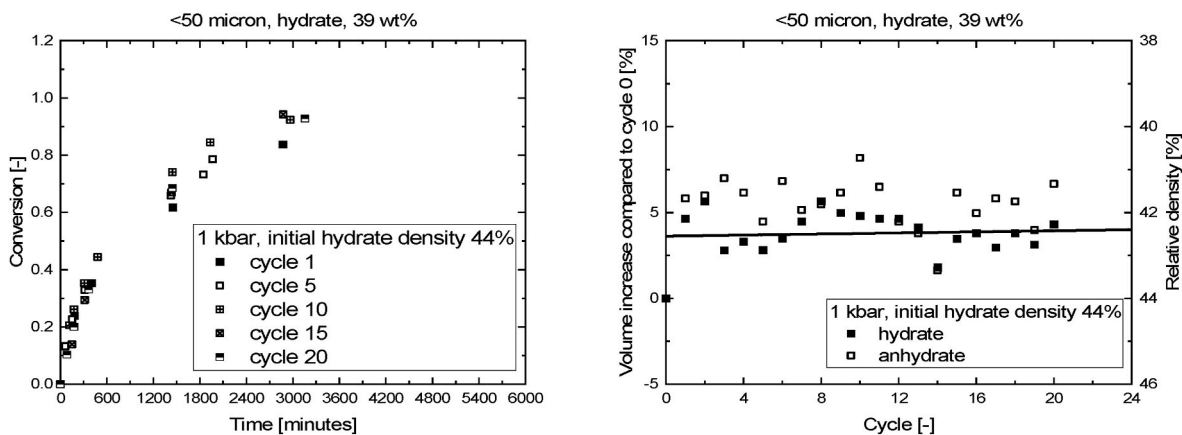


Fig. 12. Hydration conversion over time for various cycles (left) and volume increases compared to the as produced hydrate particle (right). The particle was manufactured at 1 kbar manufacturing pressures and 39 wt % binder. Hydration was performed at 33 % RH, 20 °C and dehydration overnight in an oven at 160 °C. The initial density represents the relative salt density as produced. The black line represents the linear fits through the sample in hydrated state (black squares). The absolute error in density measurements is estimated to be 0.01 [-] (1 % when the density is expressed in percentages).

To be able to compare the particle performance in between cycles and different materials an average power per volume at 50 % conversion $P_{50\%}$ [$\text{W} \cdot \text{m}^{-3}$] has been calculated as follows

$$P_{50\%} = \frac{N_{\text{water}} \cdot \Delta H}{t_{50\%} \cdot V} \quad [3]$$

Here N_{water} [mol] represents the reacted moles of water at 50 % conversion, $t_{50\%}$ [s] the time it takes to reach 50 % conversion, ΔH [$\text{J} \cdot \text{mol}^{-1}$] the reaction enthalpy and V [m^3] the total volume of the particle at a given cycle. The reaction enthalpy is calculated from theoretical literature values to be $\Delta H^* = 63.6 \text{ kJ} \cdot \text{mol}^{-1}$ [28,29]. It is assumed that enthalpy variations over cycling or hydration conversion are negligible.

The average power at 50 % conversion for the samples from Fig. 9 is given in Fig. 10.

From Fig. 10 it is visible that the power output per volume for both samples increases with cycling, indicating that the increase in kinetics outweighs the effect of volume increase with cycling. The values for the 8 wt % binder sample are lower compared to the 5 wt % sample due to the higher amount of binder (less salt hydrate) and slightly slower kinetics. In addition to that the first cycle power output is lower as what is predicted for the first cycle from non-stabilized particles (green line in Fig. 10) [23]. This indicates that the PDMS binder during cycle 1 slows down particle hydration.

When the power output is plotted against the relative density, a linear trend of increase in power with decreasing particle density is observed. This observation matches with earlier observation made for non-stabilized particles [23].

3.4. CaC_2O_4 - PDMS: Cyclic hydration kinetics and particle performance

For successful stabilization of $\text{CaC}_2\text{O}_4 \cdot \text{H}_2\text{O}$ at least 39 wt % binder is required. Lower binder concentrations resulted in disintegration after the first dehydration. The SEM images show the small powder size, therefore high PDMS concentration was required to cover all grains (Fig. 11).

Despite the high binder concentration, still a volumetric energy density of $0.67 \text{ GJ} \cdot \text{m}^{-3}$ can be obtained based on a reaction enthalpy of $72.4 \text{ kJ} \cdot \text{mol}^{-1}$ of water [28]. Cyclic hydration kinetics and volume changes are given in Fig. 12.

It is observed that no significant kinetic acceleration occurs with cycling as well as no significant volume changes are observed. Only during the first cycle, a volume increase of around 5 % is observed which remains furthermore unchanged over cycling. Consequently, no additional porosity is created which would aid water vapor transport

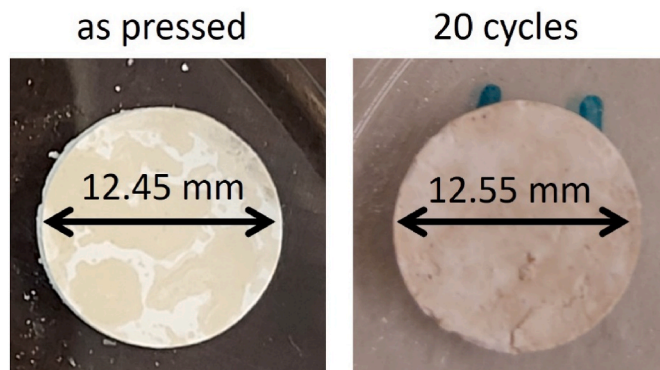


Fig. 13. Particle made from $<50 \mu\text{m}$ powder at 1 kbar manufacturing pressures and 39 wt % binder before cycling (as pressed) and after 20 dehydration/hydration cycles.

enhancing kinetics, as is the case in K_2CO_3 PDMS composites (Fig. 9). As a result, a constant average power output at 50 % conversion over cycling of $5 \pm 1 \text{ kW} \cdot \text{m}^{-3}$ is obtained.

The low swelling of the composite is inherent to the use of CaC_2O_4 . CaC_2O_4 has a crystal density of $2.22 \text{ g} \cdot \text{cm}^{-3}$ and $1.97 \text{ g} \cdot \text{cm}^{-3}$ when in monohydrate and anhydrous state, respectively [10,11]. In contrast to other salt hydrates, the hydrate density is higher compared to the anhydrous density. This is due to the minimal volume changes in the crystal lattice during dehydration while losing mass through removal of a hydrate water molecule. Due to the layered structure of CaC_2O_4 , and minimum volume changes in the crystal lattice during dehydration, dehydration results in void spaces within the anhydrous material. These void spaces can be filled during hydration without inducing significant crystal volume changes [30].

Visual inspection shows the good mechanical stability, apart from minor surface cracks, and minor swelling (Fig. 13).

4. Conclusion

Particles containing an internal flexible polymeric network (matrix) were fabricated using PDMS as internal stabilizer. The method presented in this work consists of a one pot fabrication step and therefore reduces the fabrication costs of the material. Due to the uniaxial compression method high energy densities can be obtained.

For K_2CO_3 the longest cyclic lifetime was obtained using 8 wt % binder, 50–300 μm powder and 1 kbar of manufacturing pressure,

having an energy density of $1.14 \text{ GJ} \bullet \text{m}^{-3}$. A reduction in volume increase per cycle was observed and mechanical cyclic stability was obtained for at least 35 cycles. The cyclic lifetime is expected to be 45–50 cycles, based on the disintegration of other particles. Kinetics accelerated with cycling and so did the average power output at 50 % conversion which both stabilize after 20 cycles at $50 \text{ kW} \bullet \text{m}^{-3}$.

Due to the low solubility of CaC_2O_4 in most solvents, impregnation methods to stabilize salt hydrates cannot be used. In addition, fabrication into cyclically stable mm-sized particles is difficult. With the developed technology, a successful CaC_2O_4 -PDMS composite is fabricated with an energy density of $0.67 \text{ GJ} \bullet \text{m}^{-3}$. Mechanical stabilization was achieved using 39 wt %. binder. For the CaC_2O_4 -PDMS composite a single swelling step occurred during the first cycle after which the dimensions of the particles remained constant. As a result, stable kinetics was already observed after the first cycle and the average power output at 50 % conversion with cycling remained constant at $5 \text{ kW} \bullet \text{m}^{-3}$. Mechanical stability for at least 20 cycles was observed. To the knowledge of the authors, the manufactured $\text{CaC}_2\text{O}_4 \cdot \text{H}_2\text{O}$ -PDMS composite is the first composite of CaC_2O_4 suitable for heat battery application.

The results from this work show how a one-pot fabrication method can be used to obtain mm-sized mechanically stable particles. The developed method can be used for two main purposes. First, to mitigate the well known stability issues associated with salt hydrates. Second, aid in the manufacturing of mm-sized particles of salt hydrates which, until now, have not been manufactured due to material properties.

Funding

This publication is part of the Mat4Heat project with project number 739.017.014 of the research program Mat4Sus which is financed by the Dutch Research Council (NWO).

Notes

The authors declare no competing financial interest.

CRediT authorship contribution statement

Joey Aarts: Conceptualization, Methodology, Writing – original draft, Visualization, Investigation. **Bas van Ravensteijn:** Conceptualization, Writing – review & editing. **Hartmut Fischer:** Conceptualization, Writing – review & editing. **Olaf Adan:** Conceptualization, Writing – review & editing, Supervision, Funding acquisition. **Henk Huinink:** Conceptualization, Writing – review & editing, Supervision, Funding acquisition.

Declaration of competing interest

The authors declare that they have no known competing financial interests or personal relationships that could have appeared to influence the work reported in this paper.

Data availability

Data will be made available on request.

Acknowledgements

The authors would like to thank Hans Dalderop for his technical support. Evonik Functional Solutions GmbH is thanked for providing the potassium carbonate salt.

References

- [1] Heating – Analysis - Iea. <https://www.iea.org/reports/heating>. [Accessed 10 January 2023].
- [2] Michel B, Mazet N, Mauran S, Stitou D, Xu J. Thermochemical process for seasonal storage of solar energy: characterization and modeling of a high density reactive bed. *Energy* Nov. 2012;47(1):553–63. <https://doi.org/10.1016/j.energy.2012.09.029>.
- [3] Beving MAJM, Frijns AJH, Rindt CCM, Smeulders DMJ. Effect of cycle-induced crack formation on the hydration behaviour of K_2CO_3 particles: experiments and modelling. *Thermochim Acta* Oct. 2020;692:178752. <https://doi.org/10.1016/j.tca.2020.178752>. March.
- [4] J. Aarts, H. Fischer, H. Huinink, and O. Adan, Impact of cycling on the performance of mm-sized salt hydrate particles [Manuscript submitted for publication].
- [5] Donkers PAJ, Söğütoglu LC, Huinink HP, Fischer HR, Adan OCG. A review of salt hydrates for seasonal heat storage in domestic applications. *Appl Energy* Aug. 2017;199:45–68. <https://doi.org/10.1016/j.apenergy.2017.04.080>.
- [6] Wang S, Hoes P-J, Hensen JLM, Adan OCG, Donkers PAJ. Identifying promising use cases for a novel heat battery in Dutch residential buildings. In: CLIMA 2022 Conf., no. SE-Energy; May 2022. <https://doi.org/10.34641/clima.2022.165>.
- [7] Mazur N. Boosting power of salt hydrates for heat storage. Eindhoven University of Technology; 2023.
- [8] Ben Chanaa M, Lallemand M, Bertrand G. Exploration systematique de la cinetique de rehydratation d'un sel renversable. Exemple de la reaction $\text{CaC}_2\text{O}_4(\text{s}) + \text{H}_2\text{O}(\text{g}) \rightarrow \text{CaC}_2\text{O}_4 \cdot \text{H}_2\text{O}(\text{s})$. *Thermochim Acta* Jan. 1986;97:369–85. [https://doi.org/10.1016/0040-6031\(86\)87041-1](https://doi.org/10.1016/0040-6031(86)87041-1).
- [9] Knoll C, et al. Probing cycle stability and reversibility in thermochemical energy storage – $\text{CaC}_2\text{O}_4 \cdot \text{H}_2\text{O}$ as perfect match? *Appl Energy* Feb. 2017;187:1–9. <https://doi.org/10.1016/j.apenergy.2016.11.053>.
- [10] P. Villars and K. Cenzual, Eds., “ $\text{CaC}_2\text{O}_4 \cdot \text{H}_2\text{O}$ ($\text{Ca}[\text{C}_2\text{O}_4][\text{H}_2\text{O}]$) rt Crystal Structure: Datasheet from ‘PAULING FILE Multinaries Edition – 2012’ in SpringerMaterials (https://materials.springer.com/isp/crystallographic/docs/sd_1615898).” Springer-Verlag Berlin Heidelberg & Material Phases Data System (MPDS), Switzerland & National Institute for Materials Science (NIMS), Japan, [Online]. Available: https://materials.springer.com/isp/crystallographic/docs/sd_1615898.
- [11] P. Villars and K. Cenzual, Eds., “ $\text{Ca}[\text{C}_2\text{O}_4]$, β ($\text{Ca}[\text{C}_2\text{O}_4]$) Crystal Structure: Datasheet from ‘PAULING FILE Multinaries Edition – 2012’ in SpringerMaterials (https://materials.springer.com/isp/crystallographic/docs/sd_1926702).” Springer-Verlag Berlin Heidelberg & Material Phases Data System (MPDS), Switzerland & National Institute for Materials Science (NIMS), Japan, [Online]. Available: https://materials.springer.com/isp/crystallographic/docs/sd_1926702.
- [12] van Ravensteijn BGP, et al. Encapsulation of salt hydrates by polymer coatings for low-temperature heat storage applications. *ACS Appl Polym Mater* Apr. 2021;3(4):1712–26. <https://doi.org/10.1021/acsapm.0c01186>.
- [13] Shkatulov AI, Houben J, Fischer H, Huinink HP. Stabilization of K_2CO_3 in vermiculite for thermochemical energy storage. *Renew Energy* May 2020;150 (xxxx):990–1000. <https://doi.org/10.1016/j.renene.2019.11.119>.
- [14] Zou D, Yue X, He T, Ding J, Ba D. Experimental research on the preparation of K_2CO_3 /expanded vermiculite composite energy storage material. *Materials* May 2022;15(10):3702. <https://doi.org/10.3390/ma15103702>.
- [15] Aarts J, van Ravensteijn B, Fischer H, Adan O, Huinink H. Polymeric stabilization of salt hydrates for thermochemical energy storage. *Appl Energy* Jul. 2023;341:121068. <https://doi.org/10.1016/j.apenergy.2023.121068>. March.
- [16] Salvati S, Carosio F, Saracco G, Fina A. Hydrated salt/graphite/polyelectrolyte organic-inorganic hybrids for efficient thermochemical storage. *Nanomaterials* Mar. 2019;9(3):420. <https://doi.org/10.3390/nano9030420>.
- [17] Kallenberger PA, Posern K, Linnow K, Brieler FJ, Steiger M, Fröba M. Alginate-derived salt/polymer composites for thermochemical heat storage. *Adv. Sustain. Syst.* Jul. 2018;2(7):1700160. <https://doi.org/10.1002/adsu.201700160>.
- [18] Reynolds J, Williams R, Elvins J, Jewell E, Searle J, Ke X. Development and characterisation of an alginate and expanded graphite based composite for thermochemical heat storage. *J Mater Sci* Apr. 2023;58(13):5610–24. <https://doi.org/10.1007/s10853-023-08370-1>.
- [19] Brancato V, et al. $\text{MgSO}_4 \cdot 7\text{H}_2\text{O}$ filled macro cellular foams: an innovative composite sorbent for thermo-chemical energy storage applications for solar buildings. *Sol Energy* Oct. 2018;173:1278–86. <https://doi.org/10.1016/j.solener.2018.08.075>. August.
- [20] Calabrese L, Palamara D, Piperopoulos E, Mastronardo E, Milone C, Proverbio E. Deviceful LiCl salt hydrate confinement into a macroporous silicone foam for low-temperature heat storage application. *J. Sci. Adv. Mater. Devices* Sep. 2022;7(3):100463. <https://doi.org/10.1016/j.jsamd.2022.100463>.
- [21] Gale BK, et al. Low-cost MEMS technologies. In: Reference module in materials science and materials engineering, no. July 2015. Elsevier; 2016. p. 1–32.
- [22] Bian P, Wang Y, McCarthy TJ. Rediscovering silicones: the anomalous water permeability of ‘hydrophobic’ PDMS suggests nanostructure and applications in water purification and anti-icing. *Macromol Rapid Commun* Mar. 2021;42(5):2000682. <https://doi.org/10.1002/marc.202000682>.
- [23] Aarts J, et al. Diffusion limited hydration kinetics of millimeter sized salt hydrate particles for thermochemical heat storage. *J Energy Storage* Mar. 2022;47:103554. <https://doi.org/10.1016/j.est.2021.103554>. November 2021.
- [24] Greenspan L. Humidity fixed points of binary saturated aqueous solutions. *J. Res. Natl. Bur. Stand. Sect. A Phys. Chem.* Jan. 1977;81A(1):89. <https://doi.org/10.6028/jres.081A.011>.
- [25] P. Villars and K. Cenzual, Eds., “ $\text{K}_2\text{CO}_3 \cdot 1.5\text{H}_2\text{O}$ ($\text{K}_4[\text{CO}_3]_2[\text{H}_2\text{O}]_3$) Crystal Structure: Datasheet from ‘PAULING FILE Multinaries Edition – 2012’ in SpringerMaterials (https://materials.springer.com/isp/crystallographic/docs/sd_0377610).” Springer-Verlag Berlin Heidelberg & Material Phases Data System (MPDS), Switzerland & National Institute for Materials Science (NIMS), Japan,

- [Online]. Available: https://materials.springer.com/isp/crystallographic/docs/sd_0377610.
- [26] P. Villars and K. Cenzual, Eds., "K₂CO₃ (K₂[CO₃] rt mon 1) Crystal Structure: Datasheet from 'PAULING FILE Multinaries Edition – 2012' in SpringerMaterials (https://materials.springer.com/isp/crystallographic/docs/sd_1215403).", Springer-Verlag Berlin Heidelberg & Material Phases Data System (MPDS), Switzerland & National Institute for Materials Science (NIMS), Japan, [Online]. Available: https://materials.springer.com/isp/crystallographic/docs/sd_1215403.
- [27] Meille S, Lombardi M, Chevalier J, Montanaro L. Mechanical properties of porous ceramics in compression: on the transition between elastic, brittle, and cellular behavior. *J Eur Ceram Soc* Nov. 2012;32(15):3959–67. <https://doi.org/10.1016/j.jeurceramsoc.2012.05.006>.
- [28] Wagman DD, et al. The NBS tables of chemical thermodynamic properties: selected values for inorganic and C1 and C2 organic substances in SI units. *J Phys Chem Ref Data* 1982. <https://doi.org/10.18434/M32124>.
- [29] Glasser L. Thermodynamics of inorganic hydration and of humidity control, with an extensive database of salt hydrate pairs. *J Chem Eng Data* Feb. 2014;59(2): 526–30. <https://doi.org/10.1021/je401077x>.
- [30] Izatulina AR, Gurzhiy VV, Krzhizhanovskaya MG, Kuz'mina MA, Leoni M, Frank-Kamenetskaya OV. Hydrated calcium oxalates: crystal structures, thermal stability, and phase evolution. *Cryst Growth Des Sep*. 2018;18(9):5465–78. <https://doi.org/10.1021/acs.cgd.8b00826>.